

MODELLING OF OIL FLOW COMPONENTS BETWEEN THE TANK AND ACTIVE PART OF NON-OD LIQUID-IMMERSED POWER TRANSFORMERS

*Anastasija POPOVIC¹, Zoran RADAKOVIC^{*1}, Dario ROGORA², Luca LOMBINI²*

¹University of Belgrade, School of Electrical Engineering, Bulevar kralja Aleksandra 73, Belgrade 11120, Serbia

²Tamini Trasformatori S.R.L., Viale L. Cadorna, 56a, 20025 Legnano MI, Italy

* Corresponding author; E-mail: radakovic@etf.bg.rs

The paper deals with important details of a detailed thermal hydraulic network model, a prevailing approach in building transformer thermal design tools. Oil flow components in a space between the tank and the transformer's active parts are explored using FEM CFD. These flows can significantly influence the overall temperature distribution in transformers with OF-cooling and ON-cooling with highly positioned radiators. Two heat run tests on a real OFAF transformer 125 MVA, 150 / 36 kV with different cooling arrangements (coolers of rated power 250 kW and 320 kW) are used for the analysis and experimental validation. The paper considers three oil flow components between the active part and the tank: oil by-pass, oil near the tank with losses generated due to the stray flux, and oil near the outer winding with no cylinder on its outer surface. 2D axisymmetric FEM CFD simulations pointed out that frictional pressure drop in oil by-pass is equal to zero. Recommendations for modeling the three oil flow components in THNM are proposed. The influence of the insulation bulging on the oil flow and temperatures is investigated. The bulging was evaluated based on the heat run test result with the 250 kW cooler. After such calibration, temperatures were calculated for the case of 320 kW cooler, and the THNM results were compared with the heat run test.

Key words: Finite element analysis, Detailed thermal-hydraulic network model, Power transformers, Hot-spot temperature, By-pass oil flow, Bulging

1. Introduction

Due to the losses caused by the current through the windings and magnetic flux in the core, the temperatures in the transformers rise. The temperatures must remain within the permitted limits for the applied liquid and solid insulation classes to avoid accelerated aging. During the design process, it should be ensured that the temperatures in a rated loaded transformer are below the specified limits. Transformer thermal characteristics are checked in a standard heat run test [1].

A detailed thermal hydraulic network model (THNM) has become a prevailing approach in building transformer thermal design tools. It describes heat transfer and hydraulic phenomena to a great extent. The

execution time of a calculation is appropriate. FEM CFD models the physics more in detail, but performing the simulation requires a long time, and there are often issues with convergence. FEM CFD is a convenient approach for the reduced-order modeling (ROM). Examples of such ROM are developing simple equations for split / join pressure drops in zig-zag windings [2], convection heat transfer coefficient in ducts of zig-zag winding [3], and axially and radially cooled windings without oil guiding [4]. These equations can be used to improve the accuracy of THNM.

THNM uses hydraulic and thermal networks. Using hydraulic networks, the global oil distribution between transformer parts (windings, core, oil inside the tank and outside the active part, oil in the outer cooling) and the oil flow distribution inside transformer parts are determined [5]. Using thermal networks, the temperatures of each conductor and core sheet are determined. Global oil distribution is determined through a numerical iterative process, whereby the pressure drop in each of the parts is determined by solving the detailed hydraulic network of that part [6].

The hydraulic network describing global oil distribution contains the branches representing stated transformer parts. The model assumes the oil flowing through the branches absorbs only the losses generated within the corresponding part. Once the oil exits the parts, it mixes with other flow components. The insulation cylinders prevent noticeable heat exchange between the active parts (core/windings). Thus, the stated separate consideration of heat transfer in the core and windings is justified. The conclusions about the flow in the space between the outer winding, with no cylinder on its outer surface, and the tank cannot be made so straightforward. Modeling this part of the construction is a matter of study in the paper.

The paper considers the case of an OF cooling since significant oil can appear through the space between the active part and the tank, influencing the total oil flow and temperature distribution. Results from [7] illustrate the qualitative differences between the OF and OD cooling.

The analysis is based on the three-phase OFAF transformer 125 MVA, 150 / 36 kV with compact oil to air cooler. The heat run tests were performed with two coolers of different rated power. In the considered case there is no cylinder over the outer winding – the existing THNM [5, 6] is built considering there is a cylinder on the outer winding, preventing the heat exchange between the outer winding and bulk oil. 2D axisymmetric FEM CFD simulations were performed to explore the oil flow distribution in a space between the active parts and the tank. Based on the results of these simulations, the recommendations for the hydraulic model in this space for the case of non-OD cooled power transformers are proposed.

The paper considers the influence of the bulging, which emerged as a significant issue in the considered case study.

2. Global distribution of oil flow

Fig. 1 illustrates global oil flow components for an OF cooling case.

Oil flow near a tank wall surface can be upward (Fig. 1) or downward, as presented in [5], depending on the value of stray flux tank losses and oil temperature rise to the ambient air. If the power from the tank to the oil is positive, the oil flows upward. Fig. 1 presents only a cross-section of the core plane, whereby it is cropped and shows only one of three phases.

4. FEM CFD model

2D axisymmetric FEM CFD model is developed with an initial motivation to explore the effects of merging components Q_{bp} and Q_{tank} and the introduction of the artificial axial cooling duct of 20 mm on the outer surface of winding, followed by an insulation cylinder.

Consideration of all influences on oil flow and temperature distribution requires building of 3D FEM CFD model of transformer construction. Execution of such a model is extremely demanding and time-consuming. The difficulties with numerical convergence of such models are also a reality. Instead of it, 2D axisymmetric FEM CFD simulations of artificial cylindrical geometry of concentric core, windings and tank are applied. The applied procedure is checked by comparing the calculated results with the values measured in the heat run test on the three-phase transformer of rated power 125 MVA.

The model geometry is presented in Fig. 2. The blue color represents oil. The model includes the heat transferred from the tank to oil. As in the real transformer, there is no cylinder over the outer surface of R winding.

The complex structure of the cooling ducts in MV and HV windings is replaced by a single cooling duct positioned at the outer end of the winding. The width of these ducts is determined to keep the pressure drops as in the real windings. First, the bottom (ϑ_{bo}) and top (ϑ_{to}) oil temperatures, oil flow through the windings (Q), and pressure drops are determined by the simulation of the complete transformer at the rated load using THNM implemented in [6]. After that, the width of the equivalent single duct was varied until the frictional pressure drop in the duct gets equal to frictional pressure drop in the winding, at input data ϑ_{bo} , ϑ_{to} and Q . The length of the single duct is equal to the winding height. The pressure drop in the duct is calculated by the basic equation for the duct [8] applied to 100 elements over the duct length. It is taken that oil temperature increases linearly along 100 elements, from the bottom oil temperature to the top oil temperature. The single duct is introduced for the winding to shorten computational time for FEM CFD simulations. It means the model is dedicated to the distribution of oil between the elements while keeping hydraulic behavior resemble to the real winding. The widths of equivalent ducts were determined for the input parameters (ϑ_{bo} , ϑ_{to} and Q , at temperature ϑ_{bo}) determined by [6], for the common bulging (see Subsection 6.2), for two different coolers:

- Cooler 250 kW: $\vartheta_{bo}=48.66$ °C, $\vartheta_{toMV}=77.13$ °C, $\vartheta_{toHV}=83.78$ °C, $Q_{MV}=3.12$ m³/h, $Q_{HV}=3.75$ m³/h
- Cooler 320 kW: $\vartheta_{bo}=43.88$ °C, $\vartheta_{toMV}=74.07$ °C, $\vartheta_{toHV}=80.96$ °C, $Q_{MV}=2.96$ m³/h, $Q_{HV}=3.57$ m³/h

The widths of the equivalent ducts for MV/HV windings amount to 10.5/9.3 mm (for 250 kW cooler) and 10.4/9.2 mm (for 320 kW cooler). The changes in the width of the equivalent single ducts in the narrow range of bottom oil temperature and oil flows, corresponding to two applied coolers, were small: for MV winding, the change was 0.94 %, and for HV winding 1.06 %. Further tests confirmed that the widths of equivalent ducts remain similar in a wider range of oil flows.

The transformer is described as 3 oil ducts (the duct between the core and the cylinder, equivalent single duct for MV winding, and equivalent single duct for HV winding). Bulk oil attaches the outer surface of R winding and the tank wall. The losses in R winding are equally distributed over its volume and for the

core, MV winding, HV winding, and the heat transferred from the tank to the oil, the losses are injected into the surfaces attaching the oil.

The insulation between the windings and the bottom and top yokes influences the flow distribution. It is included in the simplified model presented in Fig. 2. It is set considering possible oil paths and the fact that heat exchange between the insulation and the oil is practically negligible.

The input parameters for FEM CFD simulations were varied - the bottom oil temperature 0 °C, 48 °C and 70 °C, the inlet flow rate 10 m³/h, 12.5 m³/h, 15 m³/h, 17.5 m³/h, 20 m³/h, 22.5 m³/h, 25 m³/h, 27.5 m³/h and 30 m³/h. With this parametric sweep, a realistic range of input parameters is covered. It is necessary for a comprehensive study of the oil flow in the space between the active part and the tank. The widths of the equivalent ducts are set to 10.5 mm for MV winding and 9.3 mm for HV winding.

2D axisymmetric FEM CFD simulations were performed in COMSOL [9]. To test mesh dependency, simulations were performed for extra fine (one level coarser mesh than extremely fine) and extremely fine mesh (the finest available automatic mesh). Extra fine mesh consists of 116531 elements, and extremely fine of 131495 elements. No changes to the meshes generated by COMSOL were performed. The results remain almost the same. For example, for the case 0 °C and 10 m³/h, the maximum difference between mass oil flow components amounts to 0.1 % for extra fine versus extremely fine mesh, while it amounts to 2.15 % for finer mesh (two level coarser mesh than extremely fine) versus extremely fine mesh. The difference in inlet to outlet pressure amounts to 0.15 % for extra fine versus extremely fine mesh, and 0.21 % for finer mesh versus extremely fine mesh. After such a grid independence study, it was proceeded with the extra fine automatic mesh.

Based on previous experience [4], 2D FEM CFD simulations are performed as transient simulations to overcome convergence issues encountered in stationary simulations. The transient simulations were run sufficiently long to reach the steady state.

The boundary temperature condition at the bottom line of the model (inlet) is a constant temperature. The boundary flow condition, a total oil flow over the bottom line of the model, is specified. A pressure boundary condition is imposed at the top line of the model (outlet). Heat flux is applied on the lines bounding the observed element for tank, core, MV, and HV windings, represented by the equivalent duct (see Fig. 2). For R winding, heat source condition is applied. All other surfaces are considered adiabatic. The stationary Navier-Stokes equations and the continuity equation govern the motion of the fluids:

$$\rho(\mathbf{u} \cdot \nabla)\mathbf{u} = \nabla \cdot [-p\mathbf{I} + \mathbf{K}] + \mathbf{F} + \rho\mathbf{g}_a \quad (1)$$

$$\nabla \cdot (\rho\mathbf{u}) = 0 \quad (2)$$

$$\mathbf{K} = \mu(\nabla\mathbf{u} + (\nabla\mathbf{u})^T) - 2/3 \mu(\nabla \cdot \mathbf{u})\mathbf{I} \quad (3)$$

Where ρ is the fluid density, \mathbf{u} is the fluid velocity, p is the fluid pressure, \mathbf{I} is the identity matrix, \mathbf{K} is calculated by (3), \mathbf{F} represents external forces applied to the fluid, \mathbf{g}_a is gravitational acceleration, and μ is the fluid dynamic viscosity. Heat balance equation and conductive heat transfer describe the thermal field distribution:

$$\rho C_p \mathbf{u} \cdot \nabla T + \nabla \cdot \mathbf{q} = P_v \quad (4)$$

$$\mathbf{q} = -k \nabla T \quad (5)$$

where C_p is the specific heat capacity, T is the absolute temperature, q is the heat flux by conduction, P_v is the volumetric heat source, and k is the thermal conductivity.

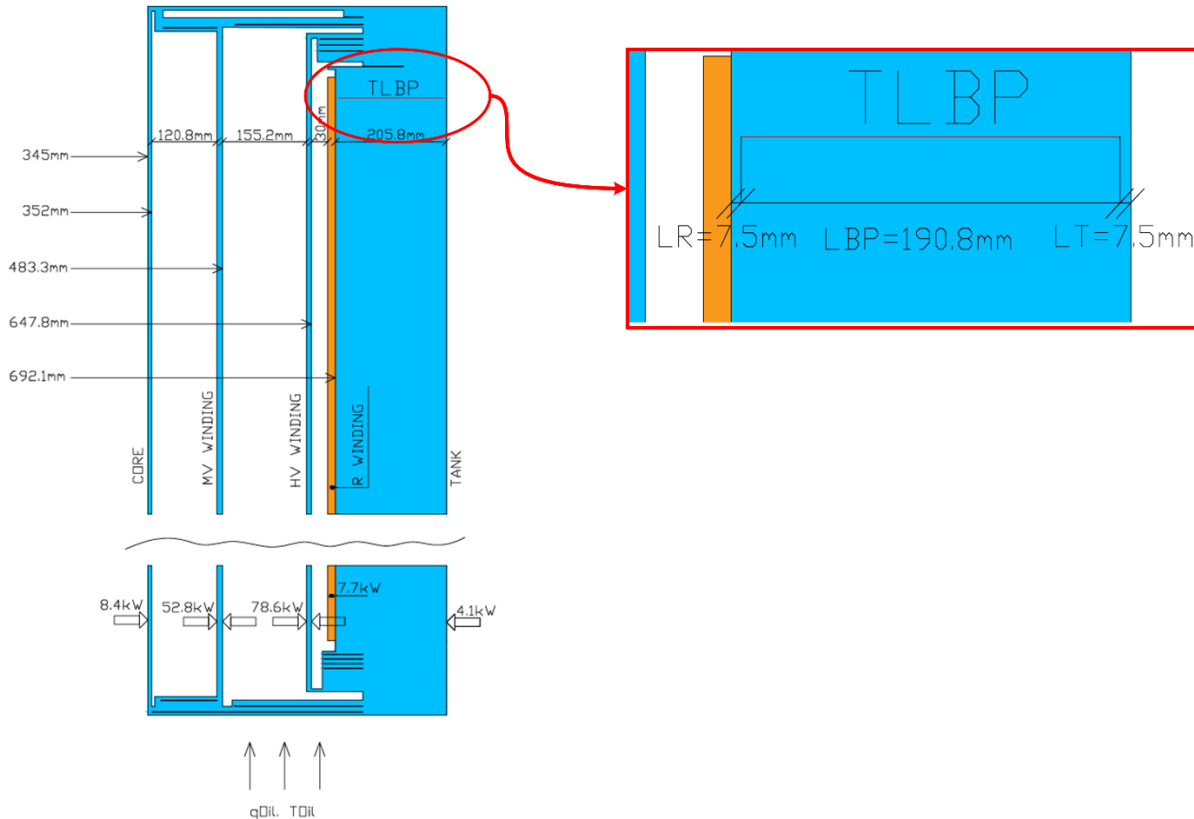


Figure 2. Model geometry used for FEM CFD simulations

5. The results of FEM CFD simulations

5.1. Details observed from FEM CFD simulations

FEM CFD simulations offer the possibility to explore details that cannot be captured by THNM.

Distribution of oil velocity and temperatures over the complete model volume are presented in Figs. 3 and 4.

The curvature of the oil streamlines appearing below and above the windings/core, presented in Fig. 5, causes a pressure drop. The pressure drop is evaluated in further analysis, showing that its influence on oil flow distribution is negligible.

As shown in Fig. 6, there is an oil temperature drop near the top of the winding equivalent cooling duct. It is caused by heat conduction and is described with the convection-diffusion equation [10]. The equation is immanently built into FEM CFD, while THNM [5] does not consider it. The temperature distribution in the oil duct influences the gravitational pressure component, thus influencing the total pressure. However, the temperature change in the small zone at the top of the duct does not noticeably affect the total gravitational pressure and, consequently, oil flow distribution.

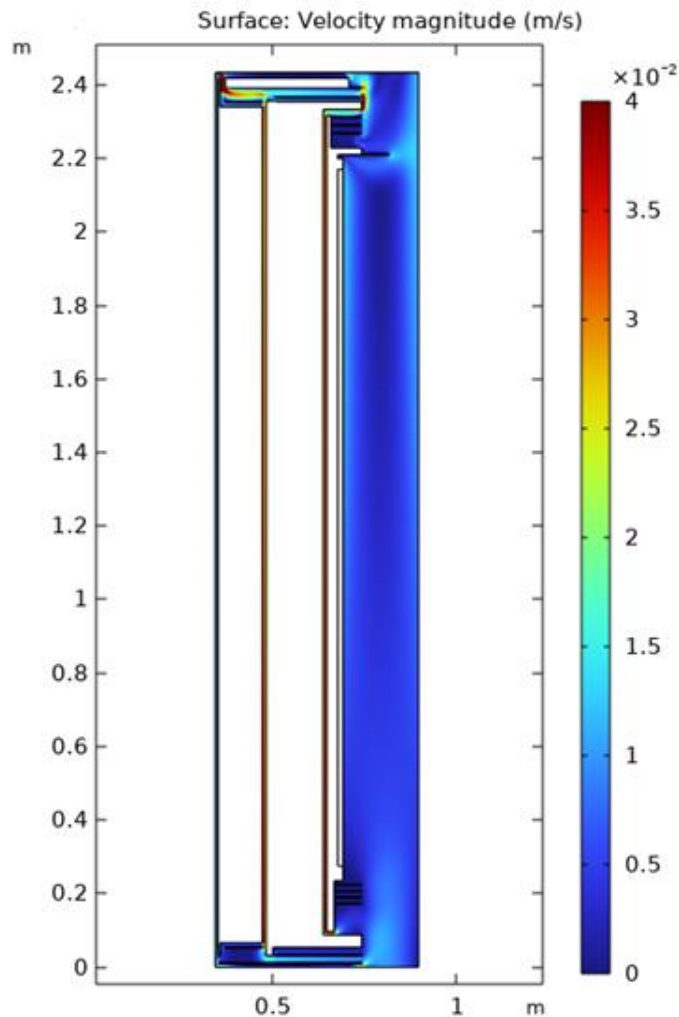


Figure 3. Oil velocity distribution for the case of the bottom oil temperature 48 °C and the inlet flow rate 25 m³/h

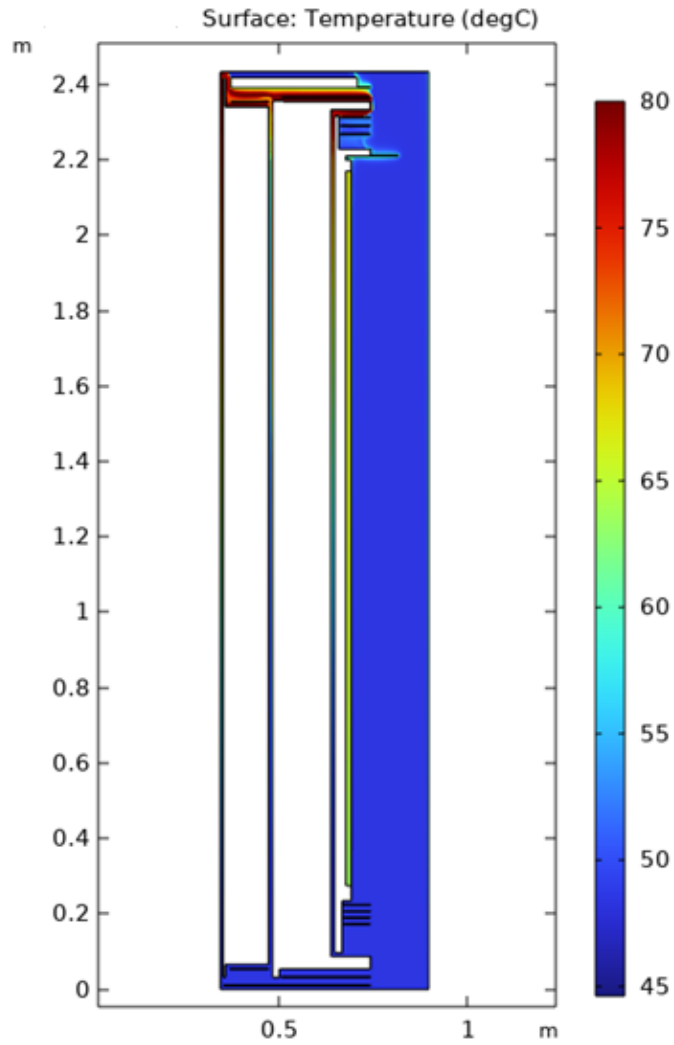


Figure 4. Temperature distribution for the case of the bottom oil temperature 48 °C and the inlet flow rate 25 m³/h

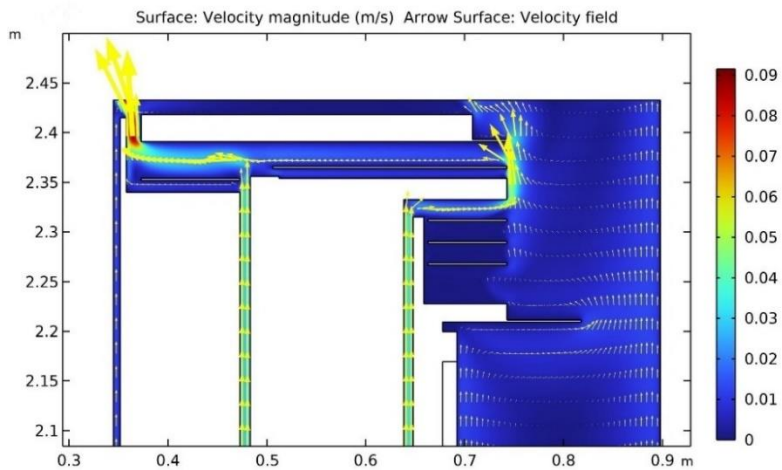


Figure 5. The curvature of the oil streamlines appearing in the zone above the windings for the case of the bottom oil temperature 48 °C and the inlet flow rate 25 m³/h

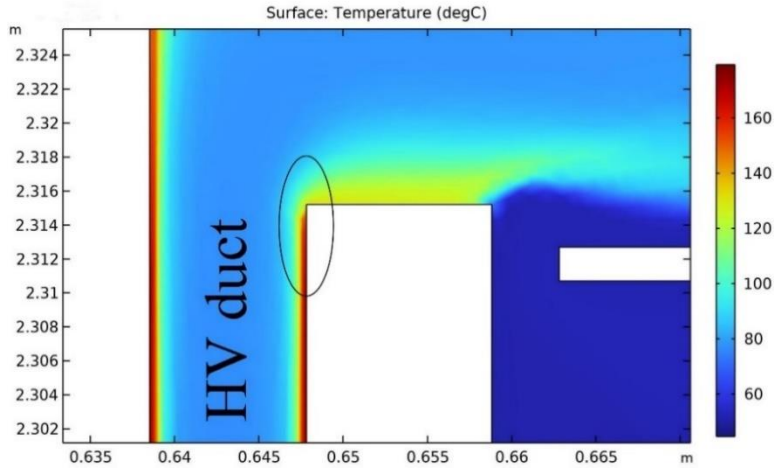


Figure 6. Temperature drop near the top of the cooling duct representing the HV winding for the case of the bottom oil temperature 48 °C and the inlet flow rate 25 m³/h

5.2. Postprocessing of FEM CFD simulations results

The FEM CFD model is built for one phase, meaning the obtained values for the winding oil flows correspond to the flows through the real windings. The by-pass/core oil flow in the transformer is equal to the by-pass/core oil flow obtained from FEM CFD multiplied by three. Pressure drops and mass oil flows were determined by postprocessing FEM CFD simulation results. The pressure drops are determined by averaging the pressures along these lines. The mass flows are determined by integrating the oil velocity axial component multiplied by density over the characteristic lines.

The characteristic lines are set as follows. The lines for R winding, oil by-pass, and oil near the tank are positioned 10 cm below the top of R winding, before the streamlines get disturbed by the insulation influence. The line for R winding is of length $LR = 7.5$ mm, positioned near R winding (TLR). The line for the tank is of length $LT = 7.5$ mm, positioned near the tank (TLT). The line for the by-pass is of length $Lbp = 205.8$ mm - LT - $LR = 190.8$ mm, positioned between the lines TLR and TLT (see line TLBP on Fig. 2). The lines for MV and HV windings and the core are positioned at the top (TLMV, TLHV, TLC, respectively) and the bottom of these elements (BLMV, BLHV, BLC, respectively), with the length equal to the width of their respective oil ducts. Two more pressures are extracted from the results of CFD simulations – the pressure at the inlet (B) and the outlet (T) of the model.

For the FEM CFD simulation at a bottom oil temperature 0 °C, a value of 10 mm was taken for LT and LR instead of 7.5 mm. These 7.5 mm and 10 mm widths correspond to the fully developed boundary layer width identified in the results of FEM CFD simulations.

5.3. Oil flow distribution between transformer parts

Parametric 2D axisymmetric FEM CFD simulations were performed for different values of inlet oil flows and temperatures, as specified in Section 4. Mass oil flows through the core, HV and MV windings were integrated over the lines BLC, BLHV, and BLMV, respectively and oil flows through the R winding

and near the tank over the lines TLR and TLT, respectively (see Subsection 5.2). Figs. 7 and 8 present the mass flow distribution between these elements for different inlet oil flows and bottom oil temperatures ($\vartheta_{bo}=70^{\circ}\text{C}$, $\vartheta_{bo}=48^{\circ}\text{C}$ and $\vartheta_{bo}=0^{\circ}\text{C}$).

It can be noticed that the flows through the core and the windings slightly increase with inlet oil flow in the zone of lower oil flows (right Fig. 7 illustrates this for MV and HV windings), while having almost a constant value in the rest of the observed inlet flow range. Fig. 9 provides information about oil by-pass flow for the case of bottom oil temperature $\vartheta_{bo}=70^{\circ}\text{C}$. Mass oil flow through the by-pass is integrated over the line TLBP, specified in Subsection 5.2. By-pass oil flow tends to zero at low inlet oil flow. Since no losses are injected to heat the oil by-pass, the oil by-pass temperature over the height is almost equal to the bottom oil temperature. Hence, the gravitational pressure in by-pass remains constant for a given bottom oil temperature as long as the by-pass oil flows. The total pressure in the oil by-pass is equal to the sum of gravitational and frictional pressures. The total pressure in all other branches is equal to the total pressure in oil by-pass. The oil flows through the core and the windings at a given bottom oil temperature remain constant as long as the oil by-pass exists (see Figs. 7 and 8), meaning the total pressure in the oil by-pass does not change. Consequently, the friction in oil by-pass does not change with by-pass oil flow at a given bottom oil temperature. Further analysis in Subsection 5.4 shows its value is negligible. This conclusion is presented in [11], which identifies the “transition point” where the entire oil flows through the windings, and the by-pass flow rate decreases to near zero. After further reduction of input oil flow, the flow through by-pass remains close to zero and the flow through other branches drops.

Different cooling conditions are imposed on different transformer elements. The oil in the equivalent cooling ducts cools the core, MV, and HV windings, whereas R winding and tank are cooled by bulk oil. The hydraulic resistance to oil flow through the ducts is higher than near the surface in bulk oil. Consequently, the oil flows near the tank and R winding do not get a constant value after the “transition point”, as is the case for the core, MV, and HV winding. The R winding flow changes less with the increase of inlet oil flow than the flow near the tank. The amount of flow through these elements depends on the generated heat, height, and position of these elements.

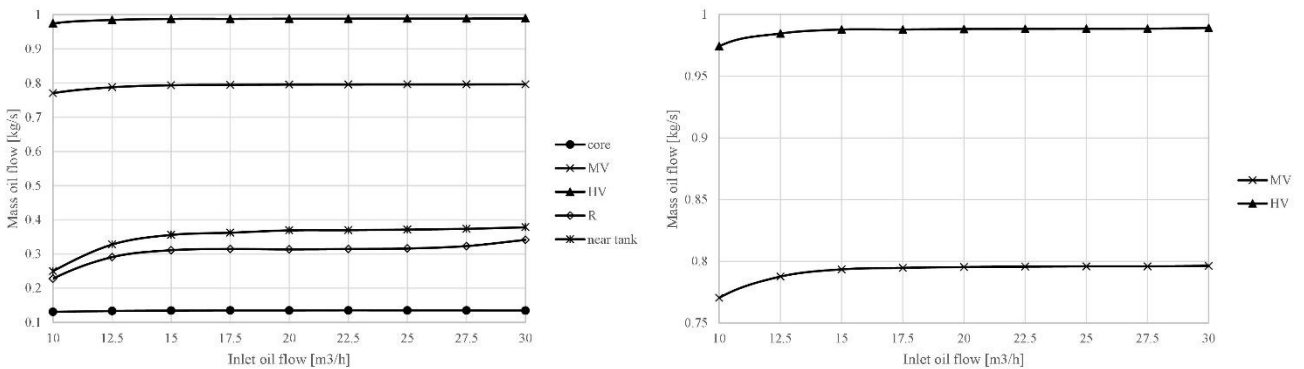


Figure 7. The mass oil flows through the core, windings and near tank at $\vartheta_{bo}=70^{\circ}\text{C}$

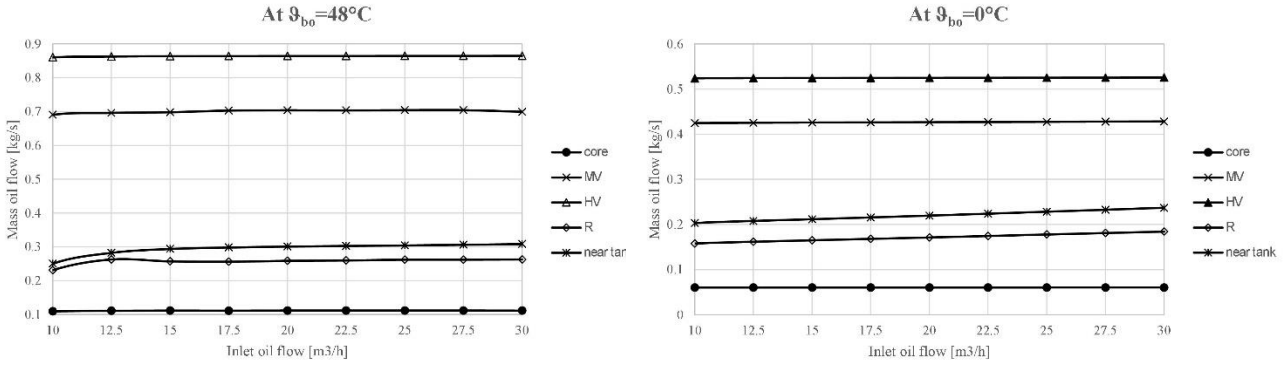


Figure 8. The mass oil flows through the core, windings and near tank

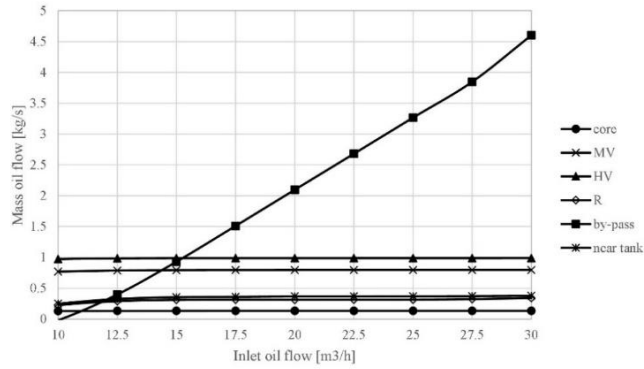


Figure 9. The mass oil flow distribution through the core, windings, near tank and by-pass for $\vartheta_{bo}=70^{\circ}\text{C}$

5.4. Pressure drop components

Table 1 presents the calculated values of frictional and gravitational pressures for the core, MV winding, and HV winding for a bottom oil temperature of 70 C. The characteristic lines used to extract the pressure drops are as follows: TLC and BLC for the core, TLMV and BLMV for the MV winding, TLHV and BLHV for the HV winding, and B and T (see Subsection 5.2). For example, the total pressure “Below the core” is determined as the difference of the pressures along the lines B and BLC, and the pressure “Above the core” as the difference of pressures along the lines TLC and T. Gravitational components (Grav) are calculated using $\rho g h$, where ρ is the oil density at the average oil temperature on the two lines bounding the observed element, g is the gravitational acceleration, h is the height of the element. Frictional pressure components (Fric) are obtained by subtracting the gravitational pressure component from the total pressure.

The pressure drops caused by the curvature of the oil streamlines above and below the windings/core are equal to the calculated frictional pressure drops in these regions. These frictional pressure drops are small compared to those along the windings/core. Its maximum value was noticed below the MV winding at a bottom oil temperature of 0 °C and an inlet oil flow 30 m³/h, and amounts to 15.75 %. Additionally, frictional pressure drops are much smaller than gravitational pressures. It should be noted that even a small

calculation error in oil temperature, and simplified calculation of the dominant gravitational pressure component, via the oil density at average oil temperature, significantly influence the frictional pressure component. This explains the negative calculated frictional pressure drops above the core, which is small and close to zero.

Table 1 – Frictional and gravitational pressure drops in the core, MV and HV windings at $\vartheta_{bo}=70\text{ }^{\circ}\text{C}$

Inlet oil flow [m ³ h- 1]	Core						MV winding						HV winding					
	Below the core		Along the core		Above the core		Below the winding		Along the winding		Above the winding		Below the winding		Along the winding		Above the winding	
	Grav [Pa]	Fric [Pa]	Grav [Pa]	Fric [Pa]	Grav [Pa]	Fric [Pa]	Grav [Pa]	Fric [Pa]	Grav [Pa]	Fric [Pa]	Grav [Pa]	Fric [Pa]	Grav [Pa]	Fric [Pa]	Grav [Pa]	Fric [Pa]	Grav [Pa]	Fric [Pa]
30	266	4.26	19675	165	148	-1.20	575	6.69	18584	167	922	3.39	808	5.89	18235	192	1004	13.3
27.5	266	4.18	19674	165	148	-1.15	575	6.59	18584	167	921	3.71	808	5.79	18235	191	1003	13.7
25	266	4.10	19674	165	148	-1.10	575	6.55	18584	167	921	4.01	808	5.65	18235	191	1003	14.0
22.5	266	4.04	19675	165	148	-1.05	575	6.41	18584	167	921	4.38	808	5.61	18235	191	1003	14.4
20	266	3.95	19674	165	148	-0.97	575	6.33	18584	166	920	4.82	808	5.53	18235	191	1002	14.9
17.5	266	3.88	19674	164	148	-0.88	575	6.33	18584	166	920	5.43	808	5.43	18235	191	1001	15.5
15	266	3.80	19674	164	148	-0.77	575	6.20	18583	166	919	6.07	808	5.30	18235	191	1001	15.2
12.5	266	3.74	19672	162	148	0.44	575	6.08	18583	165	918	6.38	808	5.28	18234	190	999	15.6
10	266	3.78	19669	158	147	0.71	575	6.04	18579	163	916	7.08	808	5.24	18232	188	998	14.4

The small values of frictional pressure drops in the zones above and below the windings/core imply that the effect of the curvatures on the oil flow distribution in the considered transformer can be neglected. Such a result is a consequence of relatively low rated voltages and insulation systems below/above the windings – there is a small number of insulation elements, resulting in a small pressure drop.

Lines B, T, and TLBP (see Subsection 5.2) are used to extract the pressures for by-pass analyses.

The frictional pressure drop along the by-pass is small compared to the total pressure drop in by-pass (the maximum value is 0.088 % at a bottom oil temperature of 70 C and an inlet oil flow 12.5 m³/h). This confirms the conclusion from [11] that the frictional pressure drop in the by-pass is zero for OF-cooled transformers.

The frictional pressure drop above the by-pass is much smaller than the total pressure drop (the maximum value is 0.85 % at a bottom oil temperature 0 °C and an inlet oil flow 10 m³/h). This means the curvature of the oil streamlines at the top of the windings does not affect the oil flow through the by-pass.

6. The results of THNM simulations

Based on the results of FEM CFD simulations presented in Subsection 5.4, the frictional pressure drop in by-pass is set to zero in THNM simulations. To investigate other issues of interest, it is supposed there is a duct and cylinder on the outer surface of R winding. Three optional widths of artificial duct are considered: 20 mm (large value, expected to resemble the most to bulk oil boundary condition), 7.5 mm (the thickness of the boundary layer at the top of R winding obtained by FEM CFD), and 6 mm (the width at which the oil flow distribution corresponds the best to the distribution obtained by FEM CFD). The simulations in Subsections 6.1, 6.2 and Section 7 were performed with duct width of 6 mm, while it has been changed in the simulations in Subsection 6.3.

6.1. Simulations with parameters adapted to FEM CFD model

In the application of THNM to an operated transformer, the losses in the tank wall are partly transferred to the ambient air and partly to the oil [6]. To keep the same total heat transferred to the oil as in FEM CFD, the losses in tank are set to zero, and the values of the losses in constructive parts, which are transferred solely to the oil, are taken as the losses value injected to the tank surface in FEM CFD simulations. These losses are set as 10 kW below and 10 kW above the windings. Two oil ducts of the width 4 mm are omitted from the core. In this way, the core is cooled only by the oil flow through the outer duct of 7 mm, as in FEM CFD simulations. The model of the core in THNM and FEM CFD remains different, since in FEM CFD the total losses in core are assigned to the limb only.

The results of FEM CFD simulations and THNM calculations, for both cooling options (coolers of 250 kW and 320 kW rated power), are presented in Table 2. The bottom oil temperatures and the total oil flows are the same in FEM CFD and THNM simulations, being obtained from THNM and used as the inputs for FEM CFD simulations. The widths of the equivalent ducts for MV/HV windings in FEM CFD simulations amounted to 10.5/9.3 mm. THNM calculations are presented for an artificial duct width of 6 mm, at which THNM and FEM CFD results align the best.

To achieve consistency between the THNM and FEM CFD results, the values of oil flow through the core and by-pass obtained from FEM CFD simulations are multiplied by three (see Subsection 5.2). Both models follow the same qualitative change in oil flows.

Table 2 – Oil flows determined by THNM simulations with input data used in FEM CFD model

Simulation	Cooler	Q_{CC} [m ³ h ⁻¹]	ϑ_{bo} [°C]	Q_C [m ³ h ⁻¹]	Q_{MV} [m ³ h ⁻¹]	Q_{HV} [m ³ h ⁻¹]	Q_R [m ³ h ⁻¹]	Q_{bp} [m ³ h ⁻¹]	Q_{tank} [m ³ h ⁻¹]	$Q_{bp} + Q_{tank}$ [m ³ h ⁻¹]	$Q_{by-pass}$ [m ³ h ⁻¹]
FEM CFD	250 kW	45.8	48.65	1.44	3.08	3.65	1.07	17.0	3.67	20.67	/
THNM	250 kW	45.8	48.65	4.66	3.12	3.75	1.42	/	/	/	16.27
FEM CFD	320 kW	42.75	43.88	1.33	2.94	3.52	1.02	15.25	3.45	18.70	/
THNM	320 kW	42.75	43.88	4.31	2.96	3.57	1.31	/	/	/	14.92

Note: Oil flows from FEM CFD simulations are obtained by dividing the mass flows with the density at the bottom oil temperature

6.2. Simulations corresponding to heat run test

The sum of the losses in the tank (P_{tank}) and construction parts below and above windings (P_{const}) at rated current determined from a short-circuit test, amounts 30 kW. In this set of simulations, they are arbitrarily set to 15 kW below and above the windings. The results of the THNM and heat run test (HRT) measurements are presented in Table 3.

Table 3 – Calculated THNM results and measurements in standard heat run test

Method	Cooler	ϑ_{amb} [°C]	θ_{to} [K]	θ_{ao} [K]	g_{MV} [K]	g_{HV} [K]	θ_{hsMV} [K]	θ_{hsHV} [K]	θ_{avgMV} [K]	θ_{avgHV} [K]
HRT	250 kW	24.9	41.5	32.8	26.1	28.7	74.2	81.6	58.9	61.5
THNM	250 kW	25	41.7	32.9	15.3	18.9	64.6	71.7	48.1	51.7
HRT	320 kW	25.9	38.9	29.1	23	25.8	68.9	76.2	52.1	54.9
THNM	320 kW	25.9	37.3	27.8	15.5	19.2	60.6	67.9	43.3	47.0

Legend: θ – temperature rise; g – gradient winding-oil; amb – ambient; to – top oil; ao – average oil; hs – hot spot; avg – average

The temperatures calculated by [6] are lower than the measured ones, indicating that the flow through the windings is lower than the calculated values. Hence, other potential reasons have been explored. It has been identified that bulging of the insulation causes a significant change in the oil flow and temperatures. It affects the hydraulic resistances in radial ducts and, consequently, the oil distribution over the pass of zig-zag cooled winding and total pressure drop over the pass. Bulging introduces additional thermal insulation to heat transfer from the conductor to the oil in radial ducts. Another temperature influence is a change in the convection heat transfer coefficients due to the change in oil flow distribution over the pass.

Values of insulation bulging in radial oil ducts of zig-zag cooled MV and HV windings, estimated using common empirical rules, are presented in Table 4. THNM simulations were performed, increasing the bulging until the calculated average and hot-spot winding temperatures in MV and HV windings get close to the measured values obtained from the heat run test with 250 kW cooler. Bulging significantly influences the calculation results but is not measured during winding manufacturing. The calibrated (increased) bulging values are presented in Table 4. The THNM simulation with so-calibrated bulging and 320 kW cooler is performed. The results, including hot-spot factor (H), are given in Table 5. The calculated hot-spot temperatures with 320 kW cooler differ from the heat run test measurements (presented in Table 2) by 0.21 K for MV winding and 3.55 K for HV winding.

Table 4 – Values of insulation bulging in radial ducts

	W	δ	w	pw	<i>bulg</i>		<i>hw=pw-bulg</i>	
					Common rules	Increased	Common rules	Increased
MV	21.26	0.4	4	3.66	0.634	0.934	2.39	1.79
HV	19.92	0.45	4	3.65	0.641	0.935	2.37	1.78

Legend: W – Width of the CTC conductor (mm), δ – Thickness of the paper insulation (mm), w – rated radial duct width (mm), pw – width of radial duct after the pressing (mm), hw – width of hydraulic radial duct (mm), *bulg* – bulging (increase of the thickness due to the conductor banding) of the insulation (mm)

Table 5 – The results obtained by THNM for different values of insulation bulging in radial ducts

Cooler	Bulg	ϑ_{amb} [°C]	θ_{to} [K]	θ_{bo} [K]	$\theta_{to}-\theta_{bo}$ [K]	Q_{MV} [m ³ h ⁻¹]	Q_{HV} [m ³ h ⁻¹]	g_{MV} [K]	g_{HV} [K]	θ_{hsMV} [K]	θ_{hsHV} [K]	H_{MV}	H_{HV}	θ_{avgMV} [K]	θ_{avgHV} [K]
250 kW	Common	25	41.7	24.0	17.6	3.18	3.82	15.2	18.9	64.6	71.7	1.51	1.59	48.1	51.7
250 kW	Increased	25	41.6	24.0	17.5	2.56	2.93	20.1	25.4	73.0	83.3	1.56	1.64	53.0	58.3
320 kW	Increased	25.9	37.2	18.3	18.9	2.44	2.80	20.5	25.9	69.1	79.7	1.56	1.64	48.2	53.7

6.3. Influence of the R winding artificial duct width

The results of THNM simulations for different widths of the artificial duct on the outer surface of R winding are presented in Table 6 for the cooler 250 kW and in Table 7 for the cooler 320 kW. Calculations were performed for the increased bulging.

The results show that the width does not affect the flows through the MV and HV windings, which have bigger hydraulic resistances. These windings are the most critical from a thermal point of view.

The width affects the flow through the R winding and, consequently, the oil by-pass flow. Typically, the outer winding without a cylinder on the outer surface is not critical from a thermal point of view. Temperatures of the R winding are presented in Table 8. Since the artificial duct width does not significantly influence the hot spot temperatures in other windings, the width of 20 mm is adopted as a common rule when modeling winding without a cylinder on the outer surface. Using the value 20 mm leads to slightly

lower flows and higher temperatures in the MV and HV windings, than using 6 mm and 7.5 mm, meaning that using 20 mm is on the safe side.

Table 9 presents the comparison of hot-spot temperature rises measured in heat run tests and calculated by [6] after applying the described calibration and adapting 20 mm as the width of the artificial duct on the outer surface of the outer winding. The data in the table represents the final benchmark of the most important (critical) temperatures obtained by the proposed methodology.

Table 6 – The influence of the width of the artificial duct on the outer surface of R winding in the case of the cooler 250 kW

Width	Q_{CC} [m ³ h ⁻¹]	ϑ_{bo} [°C]	Q_C [m ³ h ⁻¹]	θ_{hsMV} [K]	Q_{MV} [m ³ h ⁻¹]	θ_{hsHV} [K]	Q_{HV} [m ³ h ⁻¹]	Q_R [m ³ h ⁻¹]	$Q_{by-pass}$ [m ³ h ⁻¹]
6 mm	45.94	49.01	4.84	73.0	2.56	83.3	2.93	1.56	19.93
7.5 mm	45.92	49.01	4.82	73.2	2.55	83.4	2.92	2.06	18.51
20 mm	45.93	49.01	4.67	73.4	2.54	83.7	2.9	3.48	14.52

Table 7 – The influence of the width of the artificial duct on the outer surface of R winding in the case of the cooler 320 kW

Width	Q_{CC} [m ³ h ⁻¹]	ϑ_{bo} [°C]	Q_C [m ³ h ⁻¹]	θ_{hsMV} [K]	Q_{MV} [m ³ h ⁻¹]	θ_{hsHV} [K]	Q_{HV} [m ³ h ⁻¹]	Q_R [m ³ h ⁻¹]	$Q_{by-pass}$ [m ³ h ⁻¹]
6 mm	42.85	44.2	4.54	69.1	2.44	79.7	2.80	1.46	18.20
7.5 mm	42.85	44.2	4.52	68.1	2.45	79.8	2.80	1.86	17.01
20 mm	42.85	44.2	4.42	69.4	2.42	80.0	2.78	3.40	12.61

Table 8 – Calculated hot spot temperature rise of R winding

Width of the artificial duct on the outer surface of R winding	Hot spot temperature rise [K]	
	Cooler 250 kW	Cooler 320 kW
6 mm	55.76	50.71
7.5 mm	53.75	48.77
20 mm	51.17	45.59

Table 9 – Comparison of hot-spot temperatures obtained assuming the artificial duct of 20 mm on the outer surface of R winding

Cooler	θ_{hsMV} [K]		θ_{hsHVC} [K]	
	Calculated	Measured	Calculated	Measured
250 kW	73.4	74.2	83.7	81.6
320 kW	69.4	68.9	80.0	76.2

7. Conclusion

The model for oil flow distribution in OF-cooled power transformers, implemented in the software tool for thermal design based on detailed THNM, is explored. The research focused on the part between the active part and the tank. The 2D axisymmetric FEM CFD simulations and the heat run tests of a real OFAF transformer 125 MVA, 150 / 36 kV, with different cooling arrangements (coolers with rated power 250 kW and 320 kW), were used to explore the phenomena, as well as for model calibration and validation.

The concept applied in THNM considers the oil flow near the tank and the oil by-pass as a unique oil flow. This flow transfers the heat exchanged from the inner tank surfaces to the oil and the losses in

constructive parts below and above the active parts. The analyses based on FEM CFD results show that the frictional pressure drop in by-pass should be set to zero.

The concept of separating the active parts as independent inner branches of the global transformer hydraulic network can be kept. In the case transformer the outer regulating winding was without a cylinder on the outer surface, cooled by bulk oil. To preserve the concept of independent inner branches, the artificial cylinder with the 20 mm oil duct between the cylinder and the outer winding surface is recommended.

Bulging affects the pressure drops in radial oil ducts of the windings and thermal resistances to heat transfer towards the radial cooling ducts of zig-zag cooled winding. Consequently, it affects the oil flows and the oil and winding temperatures. The experience of bulging is not broadly shared in the transformer community. The THNM calculation results are given using common empirical rules for bulging and increased bulging. The increased bulging was evaluated based on the heat run test result with the cooler 250 kW and applied to the case of the cooler 320 kW. The results were compared with the heat run test results for the cooler 320 kW. The analysis presented in the paper points out that bulging estimation significantly influences temperatures in the considered case transformer. Consequently, to improve the reliability of THNM results it is recommended to measure the bulging on the produced windings and establish better rules.

Acknowledgment

This paper is a result of a research project funded by the Ministry of Education, Science and Technological Development of the Republic of Serbia (contract number 451-03-68/2022-14/200103). The research was partially conducted in the premises of the Palace of Science, Miodrag Kostić Endowment.

Nomenclature

<i>bulg</i> – bulging [m]	bo, r – oil exiting the radiators
C_p – specific heat capacity [$J \cdot kg^{-1} \cdot K^{-1}$]	bo, t – oil at tank bottom
<i>I</i> – identity matrix	bp – by-pass of oil
<i>F</i> – external forces applied to the fluid [N]	bp, t – oil at top of by-pass
<i>g</i> – gradient winding-oil [K]	const – construction parts
g_a – gravitational acceleration [$m \cdot s^{-2}$]	to – top oil
<i>H</i> – hot spot factor	tot – total
<i>h</i> – height [m]	hs – hot spot
<i>hw</i> – width of hydraulic radial duct [m]	<i>i</i> – index of active part
<i>k</i> – thermal conductivity [$W \cdot m^{-1} \cdot K^{-1}$]	oil – oil
<i>P</i> – losses [W]	rad – radiator
<i>p</i> – pressure [Pa]	tank – tank
P_v – volumetric heat source [$W \cdot m^{-3}$]	to, mix – mixed oils
<i>pw</i> – width of radial duct after the pressing [m]	to, r – oil entering radiators
<i>Q</i> – oil volumetric flow [$m^3 \cdot s^{-1}$]	to, t – oil at tank top
<i>q</i> – heat flux by conduction [$W \cdot m^{-2}$]	Abbreviations and acronyms:
<i>T</i> – absolute temperature [K]	AF – air forced
<i>u</i> – fluid velocity [$m \cdot s^{-1}$]	B – inlet
<i>W</i> – width of the CTC conductor [m]	C – core
<i>w</i> – rated radial duct width [m]	CC – compact coolers
Greek symbols:	CFD – computational fluid dynamics

δ – insulation thickness [m]	FEM – finite element method
ϑ – temperature [°C]	Fric – frictional
θ – temperature rise [K]	Grav – gravitational
μ – dynamic viscosity [kg·s·m ⁻²]	HRT – heat run test
ρ – oil density [kg·m ⁻³]	HV – high voltage
Subscripts:	MV – medium voltage
avg – average	OD – oil directed
ao – average oil	OF – oil forced
ap – active part	ON – oil natural
av – average	R – regulating winding
b – bottom	ROM – reduced-order modelling
bo – bottom oil	T – outlet
bo, mix – mixture of bottom oils	THNM – thermo-hydraulic network model

References

- [1] Standard IEC 60076-2, Power transformers – Part 2: Temperature rise for liquid-immersed transformers, Edition 3.0, 2011
- [2] Coddé, J., et al., Assessment of a hydraulic network model for zig–zag cooled power transformer windings, *Appl. Therm. Eng.*, 80 (2015), pp. 220-228
- [3] Coddé, J., et al., Improvements in heat transfer network modeling for oil-cooled power transformer winding, *11th Int. conf. on heat transfer, fluid mechanics and thermodynamics*, 2015
- [4] Popovic, A., et al., Cooling of Winding with Radial Cooling Ducts without Washers in Liquid-Immersed Power Transformers with Natural Liquid Flow, *CIGRE SC A2 and 6th International Colloquium Transformer research and asset management*, Split, Croatia, 2023
- [5] Radakovic, Z., Sorgic, M., Basics of detailed thermal-hydraulic model for thermal design of oil power transformers, *IEEE Trans. Power Delivery*, 25 (2010), 2, pp. 790-802
- [6] HoST Calculus Software, <https://www.hostcalculus.com>
- [7] Radakovic, Z., Sorgic, M., Oil-Forced Versus Oil-Directed Cooling of Power Transformers, *IEEE Trans. Power Deliv.*, 25 (2010), 4, pp. 2590–2598
- [8] Idelchik, I. E., *Handbook of Hydraulic Resistances*, Boca Raton, FL: CRC, 1994
- [9] COMSOL Multiphysics® v. 6.1. www.comsol.com. COMSOL AB, Stockholm, Sweden
- [10] Ferziger, J. H., Peric, M., *Computational Methods for Fluid Dynamics*, 3rd edition, Springer, Berlin, Germany, 2002 [5] Radakovic, Z., Sorgic, M., Basics of detailed thermal-hydraulic model for thermal design of oil power transformers, *IEEE Trans. Power Delivery*, 25 (2010), 2, pp. 790-802
- [11] Plaznik, U., et al., Theoretical Study of Liquid Flow and Temperature Distribution in OF-Cooled Power Transformers, *Energies*, 17 (2024), 3, pp. 571
- [12] Incropera, F. P., DeWitt, D. P., *Heat and Mass Transfer*, 5th edition, Wiley, New York, 2002

Paper submitted: 15.03.2025.

Paper revised: 03.05.2025.

Paper accepted: 19.05.2025.